Angular sensitivities of volume gratings for substrate-mode optical interconnects

Shun-Der Wu, Thomas K. Gaylord, Elias N. Glytsis, and Yu-Ming Wu

The angular sensitivities of slanted volume gratings (VGs) illuminated by three-dimensional (3-D) converging–diverging spherical Gaussian beams for substrate-mode optical interconnects in microelectronics are analyzed by application of 3-D finite-beam rigorous coupled-wave analysis. Angular misalignments about the z, y, and x axes that correspond to yaw, pitch, and roll misalignments resulting from manufacturing tolerances of chips are investigated. Two cases of linear polarization of the central beam of the Gaussian are considered: $\mathbf{E} \perp \mathbf{K}$ and $\mathbf{H} \perp \mathbf{K}$, where $\mathbf{K}$ is the grating vector. From worst-case manufacturing tolerances, the ranges of yaw, pitch, and roll misalignment angles are $\alpha = \pm 1.17°$, $\beta = \pm 3.04°$, and $\gamma = \pm 3.04°$, respectively. Based on these ranges of misalignment angles, the decreases of diffraction efficiencies for slanted VGs that are due to both the yaw and the roll misalignments are relatively small. However, the efficiency of substrate-mode optical interconnects achieved by slanted VGs could be reduced by 61.04% for $\mathbf{E} \perp \mathbf{K}$ polarization and by 58.63% for $\mathbf{H} \perp \mathbf{K}$ polarization because of the pitch misalignment. Thus the performance of a VG optical interconnect is most sensitive to pitch misalignment.

OCIS codes: 050.0050, 050.1950, 050.1960, 050.7330, 260.2110.

1. Introduction

Optical couplers obtained by volume gratings (VGs) have been used as substrate-mode optical interconnects[1,2] and as guided-wave optical interconnects[3–7] to overcome the performance limitations of electrical interconnects for chip-to-chip and board-to-chip interconnections. Figure 1 illustrates a physical implementation of a substrate-mode optical interconnect by use of a VG to couple an optical signal emitted by a single-mode laser into a substrate for the board-to-chip interconnection in a future gigascale integration (GSI) chip. From the viewpoint of system construction, the manufacturing tolerances and the assembly errors of the chip and the printed wiring board will result in misalignment between the incident beam and the grating coupler and therefore in the deviation of the incident angle from the designed Bragg condition. As a result, the performance of the grating coupler will degrade.

For the sensitivity analysis of a VG, Leith *et al.*[8] applied the scalar Kirchhoff diffraction integral as well as a rigorous formalism derived from Maxwell's equations to study the effects of the deviation from the Bragg condition owing to either angle or wavelength detuning on the diffraction efficiency for a thick hologram illuminated by a plane wave. Kogelnik developed the two-wave first-order coupled-wave analysis[9] also referred to as Kogelnik's analysis to calculate the diffraction efficiencies of VGs with respect to angular misalignments and wavelength detuning. Friesem and Walker,[10] Kubota,[11] and Damzen *et al.*[12] utilized Kogelnik's analysis to study the angular sensitivities of VGs illuminated by plane waves. Furthermore, Chu and Kong[13] applied modal analysis to calculate the diffraction efficiency of a periodically modulated slab medium as a function of incident angle. Chatterjee and Reagan,[14] however, applied Kogelnik's analysis in conjunction with an acousto-optic multiple scattering model to investigate the effects of angular misalignment and wavelength detuning on the performance of VGs illuminated by a plane wave and a two-dimensional (2-D) Gaussian-profile plane wave, and Wang[15] proposed an impulse-response technique in conjunction with Kogelnik's analysis to study both angular sensitivities and wavelength sensitivities of a planar VG with three-

S.-D. Wu (gte782q@prism.gatech.edu), T. K. Gaylord, and Y.-M. Wu are with the School of Electrical and Computer Engineering, Microelectronics Research Center, Georgia Institute of Technology, Atlanta, Georgia 30332. E. N. Glytsis is with the School of Electrical and Computer Engineering, the National Technical University of Athens, Athens, Greece.

Received 19 November 2004; revised manuscript received 16 February 2005; accepted 23 February 2005.

0003-6935/05/214447-07$15.00/0

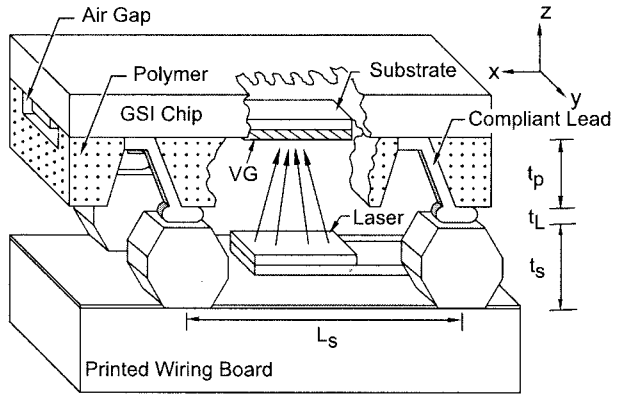

Fig. 1. Physical implementation of a substrate-mode optical interconnect utilizing a VG to couple an optical signal emitted by a single-mode laser mounted on a printed wiring board into a substrate for the board-to-chip interconnection.

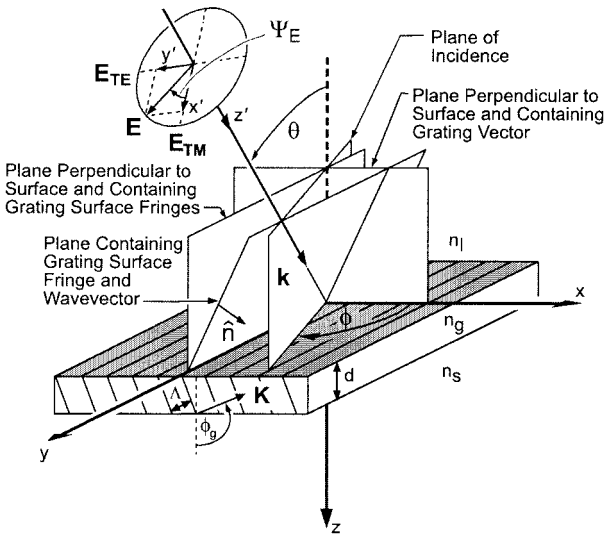

Fig. 2. Geometry of a planar VG illuminated by a converging–diverging spherical Gaussian beam with wave vector $\mathbf{k}$ at an arbitrary incident angle θ, at an arbitrary azimuthal angle ϕ, and with an arbitrary linear polarization (specified by polarization angle Ψ_E). The VG has period Λ, slant angle ϕ_g, and thickness d. The refractive indices of the incident region, the grating, and the substrate are n_I, n_g, and n_s, respectively.

dimensional (3-D) Gaussian-profile plane-wave incidence as a function of the grating-thickness-to-beam-width ratio. In general, the FWHM for the responses of both angular sensitivities and wavelength sensitivities decreases as the grating-thickness-to-beam-width ratio decreases. All these angular-sensitivity analyses were made either for plane-wave incidence or for Gaussian-profile plane-wave incidence and were restricted to the Bragg diffraction regime (i.e., only the transmitted beam and the diffracted beam were considered) and to classic diffraction geometry (i.e., the grating vector was assumed to lie in the incident plane). Recently Frantz *et al.*[16] applied conventional 3-D rigorous coupled-wave analysis[17] (RCWA) in conjunction with Monte Carlo simulation to investigate the transmittance of a noise VG as a function of the reconstruction angle (i.e., the incident angle) for 3-D conical diffraction; however, in this analysis the incident beam was assumed to be a plane wave.

For practical applications, the incident beam emitted by a single-mode laser closely approximates a 3-D converging–diverging spherical Gaussian beam, and generally the incident wave vector does not lie in the plane perpendicular to the grating surface that contains the grating vector. This configuration produces 3-D conical diffraction. Therefore, in this paper we investigate, for the first time to the authors' knowledge, the angular sensitivities of a planar VG illuminated by a 3-D converging–diverging spherical Gaussian beam at an arbitrary incident angle, at an arbitrary azimuthal angle, and with any linear polarization. The analysis utilizes 3-D finite-beam (FB) RCWA.[18] The effects of angular misalignments about the z, y, and x axes, which correspond to yaw, pitch, and roll misalignments, respectively, on the diffraction efficiencies of planar VGs are investigated. In Section 2 the general geometry for the 3-D conical diffraction of a planar VG, the configurations of yaw, pitch, and roll misalignments, and the numerical method are briefly introduced. In Section 3 the effects of yaw, pitch, and roll misalignments on the diffraction efficiencies of a substrate-mode optical interconnect achieved by a slanted VG are presented. The two cases of linear polarization of the central beam of the Gaussian ($\mathbf{E} \perp \mathbf{K}$ and $\mathbf{H} \perp \mathbf{K}$) are investigated. Finally, the primary results are summarized in Section 4.

2. Analysis Method

A. Geometry of Conical Diffraction for a Volume Grating

Figure 2 shows the general geometry of 3-D conical diffraction by a planar VG.[18] The planar VG with thickness d has an arbitrary direction of the periodicity of the dielectric constant on the $x-z$ plane. Therefore a VG with grating period Λ and slant angle ϕ_g can be characterized by a periodic dielectric constant expandable in a Fourier series as

$$\varepsilon = \varepsilon_0 + \sum_{p=1}^{\infty} \varepsilon_p{}^c \cos(p\mathbf{K}\cdot\mathbf{r}) + \sum_{p=1}^{\infty} \varepsilon_p{}^s \sin(p\mathbf{K}\cdot\mathbf{r}), \quad (1)$$

where $\varepsilon_0 = n_g{}^2$ is the average dielectric constant, $\varepsilon_p{}^c$ and $\varepsilon_p{}^s$ are the pth harmonics of the dielectric constant, $\mathbf{K} = (2\pi/\Lambda)(\hat{x}\sin\phi_g + \hat{z}\cos\phi_g)$ is the grating vector, and $\mathbf{r} = x\hat{x} + z\hat{z}$ is the position vector.

The 3-D converging–diverging spherical Gaussian beam with any linear polarization orientation specified by polarization angle Ψ_E propagates along the z' direction [in the beam-coordinate system (x', y', z')] and is obliquely incident at an arbitrary incident angle θ and at an arbitrary azimuthal angle ϕ [in the VG coordinate system (x, y, z)] from the incident region with refractive index n_I upon a planar VG and then diffracts into the substrate region with refractive index n_s as a substrate-mode optical intercon-

nect. In addition, the Gaussian beam is assumed to be focused on the input surface of a planar VG, and therefore the electric field of the incident beam at $z' = 0$ can be represented as[18]

$$\mathbf{E}^{\text{inc}} = \exp\left\{-\left[\left(\frac{x'}{w_{0x'}}\right)^2 + \left(\frac{y'}{w_{0y'}}\right)^2\right]\right\}\hat{e}, \tag{2}$$

where $w_{0u'}$ is the beam radius at the beam waist in the $u'(u' = x', y')$ direction, and $\hat{e}$ is the polarization unit vector of the central beam, given by

$$\begin{aligned}\hat{e} &= e_x\hat{x} + e_y\hat{y} + e_z\hat{z} \\ &= (\cos\Psi_E \cos\phi \cos\theta - \sin\Psi_E \sin\phi)\hat{x} \\ &\quad + (\cos\Psi_E \cos\phi \cos\theta + \sin\Psi_E \sin\phi)\hat{y} \\ &\quad + (\cos\Psi_E \sin\theta)\hat{z}. \end{aligned} \tag{3}$$

B. Yaw, Pitch, and Roll Misalignments

As shown in Fig. 1, the separation between the VG and the laser (mounted on a printed wiring board) for a GSI chip in the z direction is determined by the sum of polymer thickness t_p, compliant-lead thickness t_L, and solder-bump height t_s. Therefore the manufacturing tolerances of these components can lead to different separations of the GSI chip at two adjacent solder-bump locations and result in vertical misalignments of a VG. As a result, the VG experiences angular misalignments about both the y axis and the x axis, which correspond to pitch and roll misalignments, respectively. Because of fabrication errors, however, the solder bumps may be arranged away from their designed locations and therefore give rise to lateral misalignments of a VG; consequently the VG experiences the angular misalignment about the z axis is related to the yaw misalignment. The Bragg condition as well as all the yaw, the pitch, and the roll misalignments with misalignment angles α, β, and γ, respectively, are summarized in Fig. 3. The positive values of misalignment angles of α, β, and γ are defined in counterclockwise rotations about the z, y, and x axes, respectively, by looking antiparallel to the axes.

To determine the ranges of the misalignment angles of α, β, and γ we assume the worst-case tolerances at two adjacent solder-bump locations (with the smallest separation at one location and the largest separation at the other). Table 1 summarizes the typical tolerance of each component for a GSI chip. The parameters of solder-bump height t_s and solder-bump pitch L_s are based on *International Technology Roadmap for Semiconductor (ITRS) 2003* (Ref. 19) for the chip-to-next-level interconnection based on flip-chip technology. According to the parameters listed in Table 1, the range of the misalignment angles about the z axis is $\alpha = \pm\sin^{-1}(2/98) = \pm 1.17°$. The ranges of the misalignments about both the y axis and the x axis are $\beta = \gamma = \pm\tan^{-1}(5.2/98) = \pm 3.04°$.

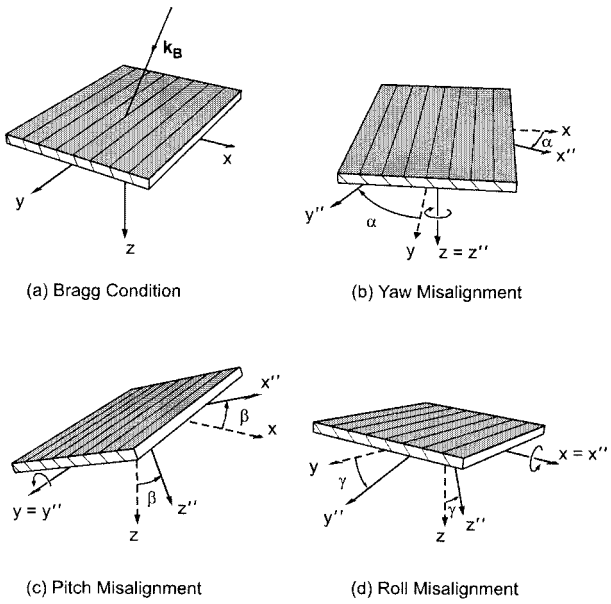

Fig. 3. Configurations of a VG at (a) the Bragg condition, (b) angular misalignment about the z axis (corresponding to yaw misalignment) by α, (c) angular misalignment about the y axis (corresponding to pitch misalignment) by β, and (d) angular misalignment about the x axis (corresponding to roll misalignment) by γ.

C. Three-Dimensional Finite-Beam Rigorous Coupled-Wave Analysis

The conventional 3-D RCWA[17] based on an important assumption that the incident beam is a plane wave is perhaps the most common method applied to analyze rigorously the 3-D conical diffraction by a grating. However, to investigate the diffraction characteristics of a VG illuminated by a finite beam such as a 3-D converging–diverging spherical Gaussian beam at conical incidence, the 3-D FB RCWA[18] derived from the conventional 3-D RCWA in conjunction with (2-D) plane-wave decomposition (PWD) is applied. The first step of 3-D FB RCWA is to determine the plane-wave spectrum of the incident beam by applying a 2-D Fourier transform. This step is also referred to as 2-D PWD. For each subbeam (i.e., each propagating component of the plane-wave spectrum) specified by an incident angle, an azimuthal angle, a polarization angle, and a plane-wave spectrum coefficient, the conventional 3-D RCWA provides the reflection wave vectors, the transmission wave vectors, and the diffraction efficiencies of the various diffracted orders. Coherently combining the conventional 3-D RCWA

Table 1. Typical Tolerance for Each Component in a GSI Chip

GSI Component	Mean Value (μm)	Tolerance (μm)
Polymer thickness (t_p)	10	±0.5
Compliant-lead thickness (t_L)	0.53	±0.1
Solder-bump height (t_s)	50	±2.0
Solder-bump pitch (L_s)	100	±1.0

results for all subbeams yields the diffracted fields and diffraction efficiencies of the various diffracted orders of a VG. The details of the 3-D FB RCWA applied for rigorous analysis of a VG illuminated by a 3-D converging–diverging spherical Gaussian beam at conical incidence are given in Ref. 18.

3. Results

For all the cases of the diffraction analyses of VGs that are investigated in this paper, a linearly polarized converging–diverging spherical Gaussian beam with beam radius $w_{0x'} = w_{0y'} = 5\ \mu$m (i.e., with a beam diameter of 10 μm) and with free-space wavelength $\lambda_0 = 850$ nm (e.g., a GaAs laser) is applied. The two cases of linear polarization of the central beam of the Gaussian of $\mathbf{E} \perp \mathbf{K}$ (i.e., the electric-field vector perpendicular to the grating vector corresponding to $\phi = 0°$ and $\Psi_E = 90°$) and $\mathbf{H} \perp \mathbf{K}$ (i.e., the magnetic-field vector perpendicular to the grating vector corresponding to $\phi = 0°$ and $\Psi_E = 0°$) are investigated. Moreover, the VG analyzed in this paper comprises an incident region with refractive index $n_I = 1.0$ (e.g., air), a substrate with refractive index $n_s = 1.55$ (e.g., benzocyclobutane), and a grating material with average dielectric constant $\varepsilon_0 = 2.25$ ($n_g = 1.5$) and modulation $\varepsilon_1^c = 0.06$ ($\Delta n_1 = 0.02$; e.g., DuPont's OmniDex613 photopolymer). The grating thickness is assumed to be $d = 10\ \mu$m. For normal incidence (i.e., $\theta = \phi = 0°$) on a slanted VG, the grating period and the slant angle are designed to provide a 45° [i.e., $\theta_1^T = 45°$ (with respect to the $+z$ axis in a counterclockwise direction)] forward-diffraction angle of the -1st propagating order to achieve multiple total internal reflections within the substrate for a substrate-mode optical interconnect (Fig. 1). Therefore, based on the first-order Bragg condition, the grating period and the slant angle of this slanted VG are $\Lambda = 711.37$ nm and $\phi_g = 113.47°$, respectively. The effects of yaw, pitch, and roll misalignments owing to manufacturing tolerances on the diffraction efficiencies are presented.

A. Yaw Misalignment

Figure 4 shows the diffraction efficiencies of the -1st forward-diffracted order, DE_{-1}^T, of a slanted VG as a function of yaw misalignment angle, α, for both central-beam $\mathbf{E} \perp \mathbf{K}$ polarization and central-beam $\mathbf{H} \perp \mathbf{K}$ polarization. In this case, incident wave vector $\mathbf{k}$ always satisfies the Bragg condition, but the polarization vector of the incident beam changes as α increases. Therefore the diffraction efficiencies are dependent only on the polarization. For example, rotating the z axis from $\alpha = 0°$ to $\alpha = -90°$ changes the polarization of the incident beam from central-beam $\mathbf{E} \perp \mathbf{K}$ polarization (i.e., the electric field points in the direction of the $+y$ axis, corresponding to TE polarization for the classic diffraction geometry) to central-beam $\mathbf{H} \perp \mathbf{K}$ polarization (i.e., the electric field points in the direction of the $+x$ axis, corresponding to TM polarization for classic diffraction geometry). As a result, DE_{-1}^T decreases as α increases toward $\pm 90°$.

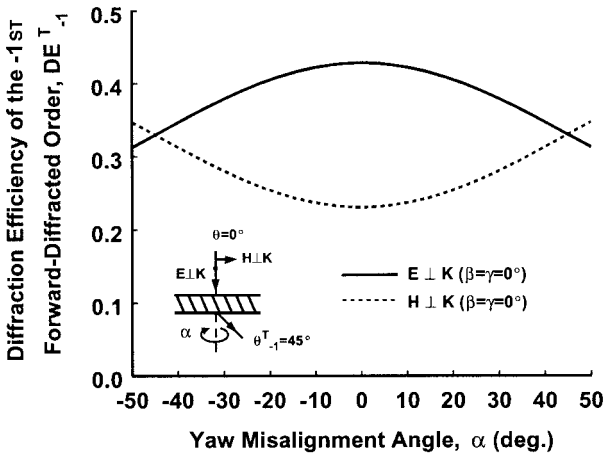

Fig. 4. Diffraction efficiencies of -1st forward-diffracted order DE_{-1}^T of a slanted VG as a function of yaw misalignment angle α for both central-beam $\mathbf{E} \perp \mathbf{K}$ polarization and central-beam $\mathbf{H} \perp \mathbf{K}$ polarization.

Similarly, the polarization of the incident beam changes from central-beam $\mathbf{H} \perp \mathbf{K}$ polarization (i.e., corresponding to TM polarization for the classic diffraction geometry) to central-beam $\mathbf{E} \perp \mathbf{K}$ polarization (i.e., corresponding to TE polarization for the classic diffraction geometry), and therefore DE_{-1}^T increases as α increases from 0° to $\pm 90°$. Note also that the diffraction efficiencies of central-beam $\mathbf{E} \perp \mathbf{K}$ polarization and central-beam $\mathbf{H} \perp \mathbf{K}$ polarization are identical at $\alpha = \pm 45°$ (Fig. 4). This result is expected because these two incident-beam–grating configurations are equivalent.

The diffraction characteristics of the five major subbeams of the 3-D converging–diverging spherical Gaussian beam (including the central subbeam, the $\pm k_x\ 1/e$ subbeams, and $\pm k_y\ 1/e$ subbeams) are shown in Fig. 5 as a function of yaw misalignment angle for

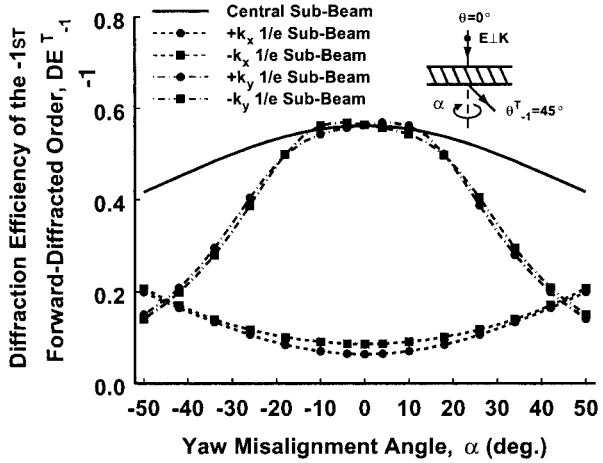

Fig. 5. Diffraction efficiencies of -1st forward-diffracted order DE_{-1}^T of a slanted VG for the central subbeam, the $\pm k_x\ 1/e$ subbeams, and the $\pm k_y\ 1/e$ subbeams of the 3-D converging–diverging spherical Gaussian beam as a function of yaw misalignment angle α for central-beam $\mathbf{E} \perp \mathbf{K}$ polarization.

central-beam $\mathbf{E} \perp \mathbf{K}$ polarization. For a normally incident beam (i.e., $\theta = \phi = 0°$) focused on a VG, the central subbeam is located at the plane-wave spectrum maximum at $k_x = k_y = 0$. The $\pm k_x$ $1/e$ subbeams and the $\pm k_y$ $1/e$ subbeams are located where the amplitude plane-wave spectra fall off to $1/e$ of the central subbeam value. As a result, the components k_x and k_y of the wave vectors for the $\pm k_x$ $1/e$ subbeams and the $\pm k_y$ $1/e$ subbeams are $k_x = \pm 2/w_{0x'} = \pm 0.4\ \mu m^{-1}$ and $k_y = 0$, and $k_x = 0$ and $k_y = \pm 2/w_{0y'} = \pm 0.4\ \mu m^{-1}$, respectively. Furthermore, for an obliquely incident Gaussian beam (i.e., $\theta \neq 0°$ and $\phi \neq 0°$), we obtain the corresponding wave vectors of the five major subbeams by incorporating the appropriate rotations of coordinate axes.[18]

As shown in Fig. 5, because the central subbeam always satisfies the Bragg condition, $DE_{-1}{}^{T}$ for the central subbeam will be dependent only on the polarization. As α increases toward $\pm 90°$, the polarization of the central subbeam changes from primarily $\mathbf{E} \perp \mathbf{K}$ polarization to primarily $\mathbf{H} \perp \mathbf{K}$ polarization, and therefore $DE_{-1}{}^{T}$ decreases. Both the $+k_y$ $1/e$ subbeam and the $-k_y$ $1/e$ subbeam almost satisfy the Bragg condition at $\alpha = 0°$, however, so the diffraction efficiencies of the $\pm k_y$ $1/e$ subbeams are close to that of the central subbeam at $\alpha = 0°$. However, as α increases toward $\pm 90°$, the $\pm k_y$ $1/e$ subbeams move away from the Bragg condition, and therefore $DE_{-1}{}^{T}$ decreases. In contrast, as both the $+k_x$ $1/e$ subbeam and the $-k_x$ $1/e$ subbeam are 3.10° away in pitch from the Bragg condition (i.e., $\theta = 3.10°$ and $\phi = 180°$ for the $+k_x$ $1/e$ subbeam and $\theta = 3.10°$ and $\phi = 0°$ for the $-k_x$ $1/e$ subbeam), the diffraction efficiencies of the $\pm k_x$ $1/e$ subbeams at $\alpha = 0°$ are much smaller than those of the central subbeam and the $\pm k_y$ $1/e$ subbeams. Furthermore, as α increases toward $\pm 90°$, the diffraction efficiencies of the $\pm k_x$ $1/e$ subbeams increase monotonically because the $\pm k_x$ $1/e$ subbeams approach the Bragg condition. Note also that $DE_{-1}{}^{T}$ of the $-k_x$ $1/e$ subbeam is larger than that of the $+k_x$ $1/e$ subbeam at $\alpha = 0°$ because the wave vector of the $-k_x$ $1/e$ subbeam is closer to the -1st forward-diffracted order.

B. Pitch Misalignment

Figure 6 shows the diffraction efficiencies of $DE_{-1}{}^{T}$ of a slanted VG as a function of pitch misalignment angle β for both central-beam $\mathbf{E} \perp \mathbf{K}$ polarization and central-beam $\mathbf{H} \perp \mathbf{K}$ polarization. As shown in Fig. 6, the behaviors of $DE_{-1}{}^{T}$ of a slanted VG with respect to β are close to that of a sinc^2 function for the small modulation case predicted by Kogelnik's analysis.[9] The FWHM for central-beam $\mathbf{E} \perp \mathbf{K}$ polarization and central-beam $\mathbf{H} \perp \mathbf{K}$ polarization of the 3-D converging–diverging spherical Gaussian beam is $\mathrm{FWHM}_{\mathbf{E}\perp\mathbf{K}} = 5.18°$ and $\mathrm{FWHM}_{\mathbf{H}\perp\mathbf{K}} = 5.27°$, respectively, i.e., larger than that of a plane wave assumed in Kogelnik's analysis [$\mathrm{FWHM}_{\mathrm{Kog}} \cong (0.86\Lambda/d)(180°/\pi) = 3.53°$]. This result is expected because a 3-D converging–diverging spherical Gaussian beam can be decomposed into various subbeams (i.e., plane-wave components). Therefore, as β increases, various k_x subbeams (i.e., the subbeams with zero wave-vector component in the y direction) of the 3-D converging–diverging spherical Gaussian beam will satisfy the Bragg condition. In contrast, for plane-wave incidence, as β increases, there are no other subbeams that will satisfy the Bragg condition. As a result, the FWHM of a 3-D converging–diverging spherical Gaussian beam is larger than that of a plane wave treated by Kogelnik's analysis.

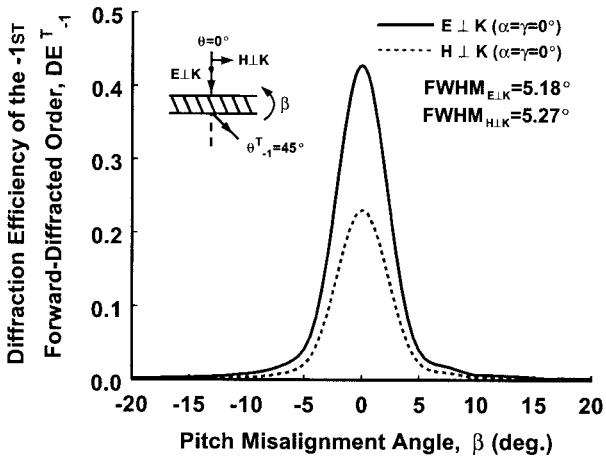

Fig. 6. Diffraction efficiencies of -1st forward-diffracted order $DE_{-1}{}^{T}$ of a slanted VG as a function of pitch misalignment angle β for both central-beam $\mathbf{E} \perp \mathbf{K}$ polarization and central-beam $\mathbf{H} \perp \mathbf{K}$ polarization.

C. Roll Misalignment

Figure 7 shows $DE_{-1}{}^{T}$ of a slanted VG as a function of roll misalignment angle γ for both central-beam $\mathbf{E} \perp \mathbf{K}$ polarization and central-beam $\mathbf{H} \perp \mathbf{K}$ polarization. As shown in Fig. 7, for small deviations of roll misalignment angle ($|\gamma| \leq 20°$) the diffraction efficiencies for both polarization cases are close to their

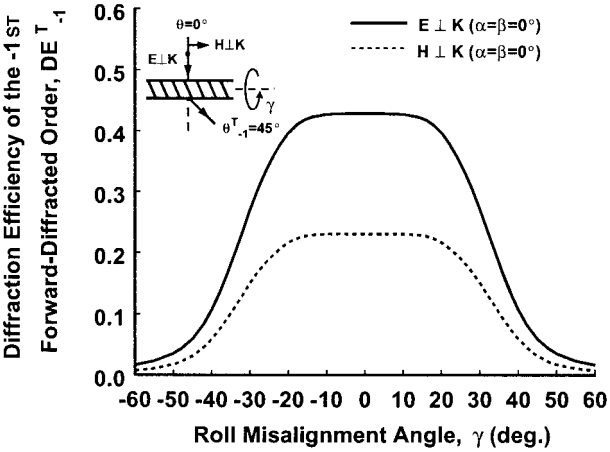

Fig. 7. Diffraction efficiencies of -1st forward-diffracted order $DE_{-1}{}^{T}$ of a slanted VG as a function of roll misalignment angle γ for both central-beam $\mathbf{E} \perp \mathbf{K}$ polarization and central-beam $\mathbf{H} \perp \mathbf{K}$ polarization.

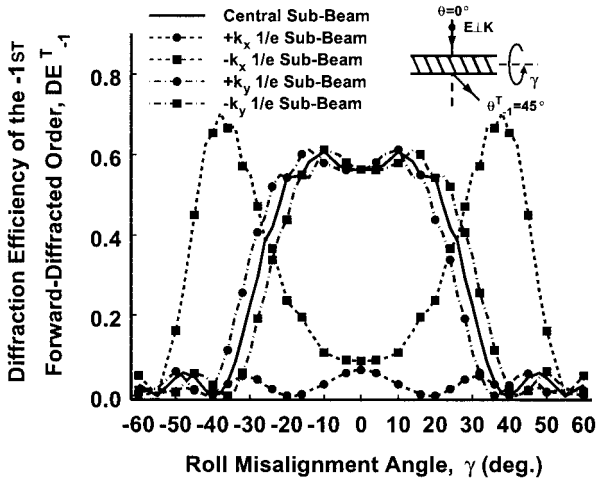

Fig. 8. Diffraction efficiencies of the −1st forward-diffracted order $DE_{-1}{}^{T}$ of a slanted VG for the central subbeam, the $\pm k_x\ 1/e$ subbeams, and the $\pm k_y\ 1/e$ subbeams of the 3-D converging–diverging spherical Gaussian beam as a function of roll misalignment angle γ for central-beam $\mathbf{E} \perp \mathbf{K}$ polarization.

corresponding values of $DE_{-1}{}^{T}$ at $\gamma = 0°$ because the central subbeams are still close to the Bragg condition and various subbeams will now satisfy the Bragg condition. However, as γ increases further ($|\gamma| > 20°$), the diffraction efficiencies decrease monotonically because all subbeams are away from the Bragg condition.

The corresponding diffraction efficiencies of the five major subbeams of the 3-D converging–diverging spherical Gaussian beam for central-beam $\mathbf{E} \perp \mathbf{K}$ polarization are shown in Fig. 8. As shown there, $DE_{-1}{}^{T}$ curves of the central subbeam, the $+k_y\ 1/e$ subbeam, and the $-k_y\ 1/e$ subbeam are identical, except that the $DE_{-1}{}^{T}$ curve of the $+k_y\ 1/e$ subbeam and the $DE_{-1}{}^{T}$ curve of the $-k_y\ 1/e$ subbeam shift by $\gamma = -3.10°$ and $\gamma = 3.10°$, respectively, from that of the central subbeam. These results are expected because all the wave vectors of $\pm k_y\ 1/e$ subbeams and the central subbeam lie on the same plane (i.e., the $y - z$ plane), except that the $\pm k_y\ 1/e$ subbeams shift from the central subbeam in roll by $\pm 3.10°$. That is, the incident angles, the azimuthal angles, and the polarization angles of both the $+k_y\ 1/e$ subbeam and the $-k_y\ 1/e$ subbeam for central-beam $\mathbf{E} \perp \mathbf{K}$ polarization are $\theta = 3.10°$, $\phi = 270°$, and $\Psi_E = 180°$ and $\theta = 3.10°$, $\phi = 90°$, and $\Psi_E = 0°$, respectively. Therefore, for $\gamma = -3.10°$ (or $\gamma = 3.10°$) rotation, the incident parameters of the $+k_y\ 1/e$ subbeam (or the $-k_y\ 1/e$ subbeam) are $\theta = 0°$, $\phi = 0°$, and $\Psi_E = 90°$, which are identical to those of the central subbeam (i.e., normally incident upon the VG) and therefore satisfy the Bragg condition. Consequently, the diffraction characteristics with respect to the $DE_{-1}{}^{T}$ curves of the $\pm k_y\ 1/e$ subbeams and the central subbeam are identical, except for the shifts of $DE_{-1}{}^{T}$ curves. As γ increases, however, the $+k_x\ 1/e$ subbeam moves away from the Bragg condition, which results in a decrease of diffraction efficiencies. However, as γ increases, the $-k_x\ 1/e$ subbeam moves close to the Bragg condition and achieves a maximum diffraction efficiency at $\gamma = \pm 36.59°$. As the roll misalignment angle increases beyond $\gamma = \pm 36.59°$, the $-k_x\ 1/e$ subbeam moves away from the Bragg condition, and therefore the diffraction efficiency decreases.

4. Summary and Discussion

Angular sensitivities of substrate-mode optical interconnects achieved by slanted volume gratings with the incident beams of three-dimensional converging–diverging spherical Gaussian beams were analyzed by application of 3-D finite-beam rigorous coupled-wave analysis based on conventional 3-D RCWA in conjunction with two-dimensional plane-wave decomposition. Two cases of linear polarization of the central beam of the Gaussian were considered: $\mathbf{E} \perp \mathbf{K}$ and $\mathbf{H} \perp \mathbf{K}$. The effects of angular misalignments about the z, y, and x axes, corresponding to as yaw, pitch, and roll misalignments, respectively, that are due to the manufacturing tolerances of microelectronic components on the diffraction efficiencies are investigated. In general, the ranges of yaw, pitch, and roll misalignment angles that are due to manufacturing tolerances are in the worst cases $\alpha = \pm 1.17°$, $\beta = \pm 3.04°$, and $\gamma = \pm 3.04°$, respectively (as discussed in Subsection 2.B). The diffraction characteristics of the central subbeam, the $\pm k_x\ 1/e$ subbeams, and the $\pm k_y\ 1/e$ subbeams with respect to angular misalignments were presented for a better physical understanding of the behavior of VGs illuminated by Gaussian beams moving away from the Bragg condition. Furthermore, it is worth mentioning that, although the angular-sensitivity analysis of VGs in this paper emphasized only a 3-D converging–diverging spherical Gaussian beam [i.e., $w_{0x'} = w_{0y'}$ defined in Eq. (2)], it can be extended to a general 3-D converging–diverging elliptical Gaussian beam of TEM_{00} mode [i.e., $w_{0x'} \neq w_{0y'}$ defined in Eq. (2)] as well as of higher orders with appropriate changes in the amplitudes and phase factors.

For normal incidence on slanted VGs that are designed for substrate-mode optical interconnects, the diffraction efficiencies depend only on the polarization of the incident beam for the yaw misalignment. As α increases toward $\pm 90°$, the diffraction efficiency decreases for central-beam $\mathbf{E} \perp \mathbf{K}$ polarization because the incident beam changes from primarily central-beam $\mathbf{E} \perp \mathbf{K}$ polarization to primarily central-beam $\mathbf{H} \perp \mathbf{K}$ polarization. In contrast, the diffraction efficiency for central-beam $\mathbf{H} \perp \mathbf{K}$ polarization increases as α increases toward $\pm 90°$ because of the change of the incident beam from primarily central-beam $\mathbf{E} \perp \mathbf{K}$ polarization to primarily central-beam $\mathbf{H} \perp \mathbf{K}$ polarization. For the pitch misalignment, the FWHMs of the diffraction efficiencies of $DE_{-1}{}^{T}$ for central-beam $\mathbf{E} \perp \mathbf{K}$ polarization and central-beam $\mathbf{H} \perp \mathbf{K}$ polarization are $\mathrm{FWHM}_{\mathbf{E}\perp\mathbf{K}} = 5.18°$ and $\mathrm{FWHM}_{\mathbf{H}\perp\mathbf{K}} = 5.27°$, respectively. For the roll misalignment the diffraction efficiencies remain almost constant as $|\gamma|$ increases from 0° (i.e., the

Bragg condition) to 20° and decrease dramatically as $|\gamma|$ increases beyond 20°. Based on the range of misalignment angles with $\alpha = \pm 1.17°$, $\beta = \pm 3.04°$, and $\gamma = \pm 3.04°$, the coupling efficiencies of the slanted VG for substrate-mode optical interconnects remain almost constant for deviations from the Bragg condition caused by both the yaw misalignment and the roll misalignment. However, the coupling efficiencies of the substrate-mode optical interconnect decrease from $DE_{-1}^{T} = 0.4284$ to $DE_{-1}^{T} = 0.1669$ (i.e., 61.04% deterioration of performance) for central-beam $\mathbf{E} \perp \mathbf{K}$ polarization and decrease from $DE_{-1}^{T} = 0.2309$ to $DE_{-1}^{T} = 0.096$ (i.e., 58.63% deterioration of performance) for central-beam $\mathbf{H} \perp \mathbf{K}$ polarization.

This research was performed as part of the Interconnect Focus Center research program supported by the Semiconductor Research Corporation, the Microelectronics Advanced Research Corporation, and the Defense Advanced Research Projects Agency.

References

1. J.-H. Yeh and R. K. Kostuk, "Substrate-mode holograms used in optical interconnects: design issues," Appl. Opt. **34,** 3152–3164 (1995).
2. J.-H. Yeh and R. K. Kostuk, "Free-space holographic optical interconnects for board-to-board and chip-to-chip interconnects," Opt. Lett. **21,** 1274–1276 (1996).
3. Q. Huang and P. R. Ashley, "Holographic Bragg grating input–output couplers for polymer waveguides at an 850-nm wavelength," Appl. Opt. **36,** 1198–1203 (1997).
4. S. M. Schultz, E. N. Glytsis, and T. K. Gaylord, "Design, fabrication, and performance of preferential-order volume grating waveguide couplers," Appl. Opt. **39,** 1223–1232 (2000).
5. R. A. Villalaz, E. N. Glytsis, and T. K. Gaylord, "Volume grating couplers: polarization and loss effect," Appl. Opt. **41,** 5223–5229 (2002).
6. S.-D. Wu and E. N. Glytsis, "Volume holographic grating couplers: rigorous analysis using the finite-difference frequency-domain method," Appl. Opt. **43,** 1009–1023 (2004).
7. S.-D. Wu, E. N. Glytsis, and T. K. Gaylord, "Optimization of finite-length input volume holographic grating couplers illuminated by finite-width incident beams," Appl. Opt. **44,** 4435–4446 (2005).
8. E. N. Leith, A. Kozma, J. Upatnieks, J. Marks, and N. Massey, "Holographic data storage in three-dimensional media," Appl. Opt. **5,** 1303–1311 (1966).
9. H. Kogelnik, "Coupled-wave theory for thick hologram gratings," Bell Syst. Tech. J. **48,** 2909–2947 (1969).
10. A. A. Friesem and J. L. Walker, "Thick absorption recording media in holography," Appl. Opt. **9,** 201–214 (1970).
11. T. Kubota, "Characteristics of thick hologram grating recorded in absorptive medium," Opt. Acta **25,** 1035–1053 (1987).
12. M. J. Damzen, Y. Matsumoto, G. J. Grofts, and R. P. M. Green, "Bragg-selectivity of a volume gain grating," Opt. Commun. **123,** 182–188 (1996).
13. R.-S. Chu and J.-A. Kong, "Modal theory of spatially periodic media," IEEE Trans. Microwave Theory Tech. **25,** 18–24 (1977).
14. M. R. Chatterjee and D. D. Reagan, "Examination of beam propagation in misaligned holographic gratings and comparison with the acousto-optic transfer function model for profiled beams," Opt. Eng. **38,** 1113–1121 (1999).
15. M. R. Wang, "Analysis and observation of finite beam Bragg diffraction by a thick planar phase grating," Appl. Opt. **35,** 582–592 (1996).
16. J. A. Frantz, R. K. Kostuk, and D. A. Waldman, "Model of noise-grating selectivity in volume holographic recording materials by use of Monte Carlo simulations," J. Opt. Soc. Am. A **21,** 378–387 (2004).
17. M. G. Moharam and T. K. Gaylord, "Three-dimensional vector coupled-wave analysis of planar-grating diffraction," J. Opt. Soc. Am. **73,** 1105–1112 (1983).
18. S.-D. Wu, T. K. Gaylord, E. N. Glytsis, and Y.-M. Wu, "Three-dimensional converging/diverging Gaussian beam diffraction by a volume grating," J. Opt. Soc. Am. A (to be published).
19. ITRS, "International technology roadmap for semiconductors 2003: assembly and packaging," http://public.itrs.net/ (2003), pp. 14–20.